*Int. J. Heat Mass Transfer.* Vol. 34, No. 10, pp. 2571–2579, 1991
Printed in Great Britain

0017–9310/91 $3.00+0.00


# Radiative energy transfer in induction plasma modelling

P. PROULX, J. MOSTAGHIMI and M. I. BOULOS
CRTP, Plasma Technology Research Center, Department of Chemical Engineering,
University of Sherbrooke, Sherbrooke, Québec, Canada J1K 2R1

(*Received* 8 *March* 1990 *and in final form* 26 *November* 1990)

**Abstract**—The influence of radiative energy losses on the flow and temperature fields of an inductively coupled radio frequency (r.f.) plasma is studied for the case of a pure argon plasma and for an argon plasma in the presence of small concentrations of copper vapor. A mathematical model is used to calculate the temperature and flow fields using different radiative source data for the plasma gas as a function of temperature. The results show that variations between different sets of data used in the computations can have a significant effect on the predicted temperature fields. The presence of small concentrations of metallic vapors is shown to be responsible for the local cooling of the plasma through the substantial increase of the radiative energy losses.

## 1. INTRODUCTION

RADIATION is one of the major mechanisms of energy loss in thermal plasmas. Radiative losses can be as high as 60% of the total energy input in a transferred arc [1, 2] and more than 40% in a radio frequency (r.f.) inductively coupled plasma [3, 4]. The significance of radiative losses depends on the operating pressure and the nature of the plasma gas. The effect is particularly important at high pressures and in the presence of metal vapors, as demonstrated in the current literature on arc-lamp technology.

The objective of the present paper is to study the role of radiative energy transfer in induction plasma modelling, and to determine the sensitivity of the computed flow and temperature fields to variations in the radiation data used.

Special attention is given to the study of the increase in radiative losses when the plasma is 'contaminated' by metallic vapors. This is often the case when metallic powders are melted in r.f. induction plasmas. The plasma gas considered is argon at atmospheric pressure.

## 2. ARGON RADIATIVE DATA

Figure 1 shows a compilation of some of the available volumetric emission data for atmospheric argon plasmas. For temperature levels below $10^4$ K, which is of interest in induction plasmas, there is a considerable scatter between the data of different authors. For example, at 7000 K, the data given by Emmons [5], curve (d) on Fig. 1, are almost two orders of magnitude larger than those of Cram [6] or Kruger [7], curves (b) and (c), respectively. Such important variations between different sources of data are bound to have a strong influence on the computed temperature field in an inductively coupled plasma.

In a number of industrial applications of thermal plasma technology, e.g. spray coating or spheroidization, metallic powders are melted and partially evaporated. The effect of contamination of argon plasmas by copper vapor on the volumetric emission of the plasma was calculated by Cram [6]. The results given in Fig. 2 show that the presence of even small concentrations of copper can cause a large increase in total radiative losses. The effect is particularly important at temperatures below $10^4$ K.

Because of the low ionization potential of copper, its presence increases the electron density by orders of magnitude at temperatures below $10^4$ K. The inelastic collisions between these electrons and the copper atoms are primarily responsible for the large increase in the line emission and consequently the increase in the total emission of the plasma.

## 3. THE MODEL

The model consists of two parts; the plasma model, and the particle trajectories and thermal history model. Due to the fact that particles act as a heat sink and cause local cooling of the plasma along their trajectories the two parts of this model are coupled. The model used here is essentially the same as described in ref. [3] and has been adopted by other investigators [8].

With respect to the plasma model, the following assumptions are made:

- Two-dimensional axisymmetric flow, temperature and concentration fields.
- One-dimensional electromagnetic fields.
- Steady, laminar flow with negligible viscous dissipation.
- Incompressible flow.

## NOMENCLATURE

| | |
|---|---|
| $A_p$ | surface area of particle |
| $B$ | magnetic field intensity |
| $C$ | particle concentration in a cell |
| $C_d$ | drag coefficient |
| $c_p$ | specific heat at constant pressure |
| $D$ | diffusion coefficient |
| $d_p$ | particle diameter |
| $E_\theta$ | circumferential electric field intensity |
| $Fr$ | body force in the radial direction |
| $g$ | acceleration of gravity |
| $h$ | enthalpy |
| $h_c$ | heat transfer coefficient |
| $H_m$ | latent heat of melting |
| $H_v$ | latent heat of evaporation |
| $H_z$ | axial magnetic field intensity |
| $J$ | current density |
| $k$ | thermal conductivity |
| $k_c$ | thermal conductivity of the quartz tube |
| $\dot{m}_p$ | power feed rate |
| $\Delta m_p$ | change in the mass of the particle |
| $N_t$ | total number of particles injected per unit time |
| $n_d$ | number of points used in the discretized particle diameter distribution |
| $n_r$ | number of discrete particle injection points used |
| $Nu$ | Nusselt number |
| $P$ | pressure |
| $P_0$ | plasma power |
| $Q$ | plasma gas flow rate |
| $Q_r$ | radiation loss per unit volume |
| $Q_p$ | energy exchange rate between the plasma and the particle during their flight in the control volume $i, j$ |
| $Q_v$ | energy needed to raise the temperature of the vapor released in the control volume from the particle temperature to that of the control volume |
| $r$ | distance in the radial direction |
| $R_0$ | inside radius of the plasma confinement tube |
| $R_c$ | coil radius |
| $Re_p$ | Reynolds number |
| $S_p^c$ | particle source term in the continuity equation |
| $S_p^E$ | particle source term in the energy equation |
| $t$ | time |
| $T$ | temperature |
| $T_a$ | ambient temperature |
| $u$ | axial velocity component |
| $U_r$ | relative speed of particles with respect to plasma gas |
| $v$ | radial velocity component |
| $V$ | volume |
| $x$ | liquid fraction of a particle |
| $y$ | particles vapor mass fraction |
| $z$ | distance in the axial direction. |

Greek symbols

| | |
|---|---|
| $\delta_w$ | tube wall thickness |
| $\varepsilon_p$ | emissivity of particle surface |
| $\mu$ | viscosity |
| $\xi$ | magnetic permeability |
| $\rho$ | density |
| $\sigma$ | electrical conductivity |
| $\sigma_p$ | standard deviation |
| $\sigma_s$ | Stefan–Boltzmann constant |
| $\tau$ | residence time of particles in a cell |
| $\chi$ | phase angle, $\phi_h - \phi_E$ |
| $\omega$ | oscillator frequency. |

Subscripts

| | |
|---|---|
| p | particles |
| $l$ | particles with initial diameter of $d_l$ |
| $k$ | particles injected at radius $r_k$ |
| $(i, j)$ | location of a typical cell. |

Superscripts

| | |
|---|---|
| $(l, k)$ | particles having an initial diameter $d_l$, and injection point $r_k$. |

- The plasma is in local thermodynamic equilibrium.
- Optically thin plasma.

It was demonstrated in ref. [9] that the one-dimensional representation of the electromagnetic fields was a valid approximation for an argon plasma under the low frequency conditions used in the present study ($f = 3$ MHz). Special attention should be given to the assumption that the plasma is optically thin in the presence of metal vapors. The question has been the subject of a separate study by Essoltani *et al.* [10] who showed that in the presence of metal vapors, iron in this case, self-absorption effects are mostly limited to a 1 mm region surrounding a source at temperatures below 12 000 K. Since this relatively short self-absorption distance is comparable with the size of the control volumes used in the temperature field modelling, one could use net radiation data to represent the radiative energy loss from a control volume, and still treat the overall plasma field as being optically thin.

The relevant equations for the plasma gas are the continuity of mass, radial and axial momentum, energy, mass diffusion and one-dimensional simplified Maxwell's equations as given in Appendix A.

With respect to the injected powders, individual particle trajectories and temperature histories are calculated, based on the following assumptions:

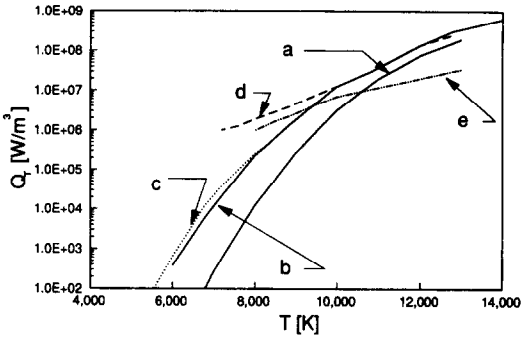


FIG. 1. Volumetric specific emission for an argon plasma at atmospheric pressure: (a) Mensing and Boedeker [12], $T < 10^4$ K, and Evans and Tankin [13], $T > 10^4$ K; (b) Cram [6]; (c) Kruger [7]; (d) Emmons [5]; (e) Kanzawa and Kimura [14].

- Particles are spherical.
- Negligible temperature gradients inside the particles.
- Particle–particle interactions are negligible.
- Drag and gravity forces are the only forces affecting the particle trajectory.
- The particles are grey body emitters.

Under typical loading conditions, the local cooling of the plasma by the injected powder is significant. Therefore, the effect of the presence of particles must be included in the plasma equations. This is achieved using the PSI-Cell model [3, 11]. In this approach, individual particle trajectories are calculated, each corresponding to a given particle diameter, injection point and injection velocity. The local cooling of the plasma is calculated as the integral of the energy exchanged between the plasma and the particles during their residence time in each control volume. The reader is referred to ref. [3] for a complete description of the governing equations, boundary conditions and the numerical technique used. The equations for the particle trajectory, thermal history and the plasma–particle coupling terms, are given in Appendix B.

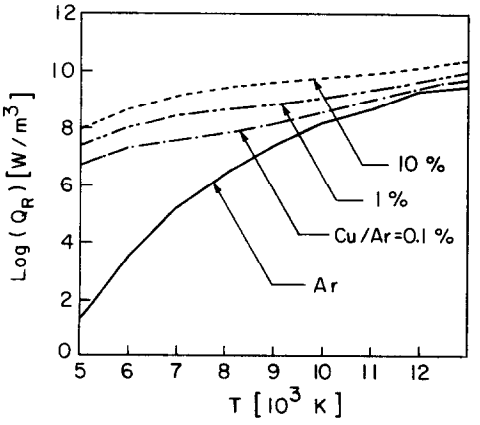


FIG. 2. Volumetric specific emission for an argon plasma in the presence of copper vapor as a function of temperature and the mass fraction of copper vapor in the mixture [6].

## 4. RESULTS AND DISCUSSION

The results of the present study are presented in two sections. The first deals with the effect of variations in the radiation data used on the calculated flow and temperature fields in the discharge. Both experimental and theoretically calculated volumetric emission data were used for that purpose, curves (a) and (b), respectively, on Fig. 1. Of the data given in Fig. 1, those represented by curve (a) are the result of experimental measurements by Mensing and Boedeker [12] for temperatures below $10^4$ K, and by Evans and Tankin [13] at temperatures above $10^4$ K. Curve (b), on the same figure, is due to theoretical calculations by Cram [6].

In the second section of this paper, the effect of the presence of metal vapors on the plasma fields is investigated using the radiation data by Cram [6] for an Ar/Cu vapor mixture as a function of temperature and composition (Fig. 2).

Figure 3 shows a schematic of the r.f. induction plasma torch. The dimensions of the torch and its operating conditions are given in Table 1. For all cases considered the net dissipated power and the induction frequency are kept constant at 5 kW and 3 MHz, respectively.

### 4.1. *Influence of radiation data*

The influence of the choice of radiation data on the calculated flow and temperature fields is presented in this section for four cases with different plasma gas (argon) flow rates, $Q_0 = 20$, 30, 40 and 50 slpm. The length of the torch is 250 mm.

Figure 4 shows typical temperature isotherms computed for a total argon flow rate of 20 slpm. The results given in Fig. 4(a) are calculated using the radiation data of Mensing and Boedeker [12] and Evans

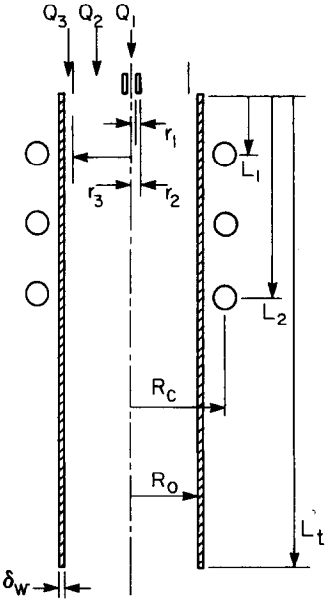


FIG. 3. Schematic of the induction plasma torch.

Table 1. Dimensions and operating conditions of the inductively coupled r.f. plasma torch

| | |
|---|---|
| $r_1$ | 1.7 mm |
| $r_2$ | 3.7 mm |
| $r_3$ | 18.8 mm |
| $R_0$ | 25.0 mm |
| $R_c$ | 33.0 mm |
| $L_1$ | 10.0 mm |
| $L_2$ | 74.0 mm |
| $L_t$ | 250–500 mm |
| $\delta_w$ | 2.0 mm |
| $P_0$ | 5 kW |
| $f$ | 3 MHz |
| $Q_1$ | 0–4.0 slpm |
| $Q_2$ | 3.0–7.5 slpm |
| $Q_3$ | 17.0–42.5 slpm |
| $Q_0$ | $Q_1+Q_2+Q_3$ |

and Tankin [13], curve (a) on Fig. 1, while Fig. 4(b) gives the results of computations carried out using the radiation data by Cram [6], curve (b) on Fig. 1. As expected, the larger radiation loss data results in an overall lower temperature field and a smaller region of the flow in which the temperature is in excess of 9000 K. It is also noted that the maximum predicted temperature differs by more than 1000 K depending on the source of radiation data used.

Figure 5 shows the corresponding energy balance on the plasma using these two sets of radiation data,

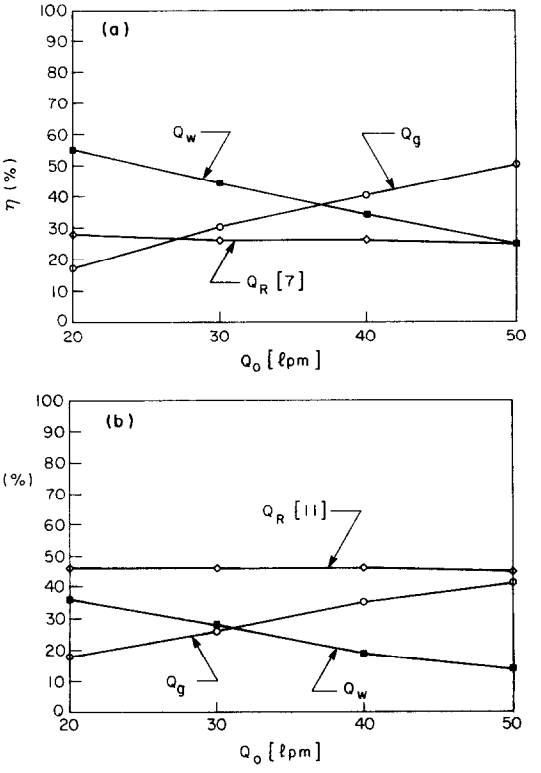


FIG. 5. Energy balance on the torch: (a) results obtained using the radiation data by Mensing and Boedeker [12] and Evans and Tankin [13]; (b) results obtained using the radiation data by Cram [6].

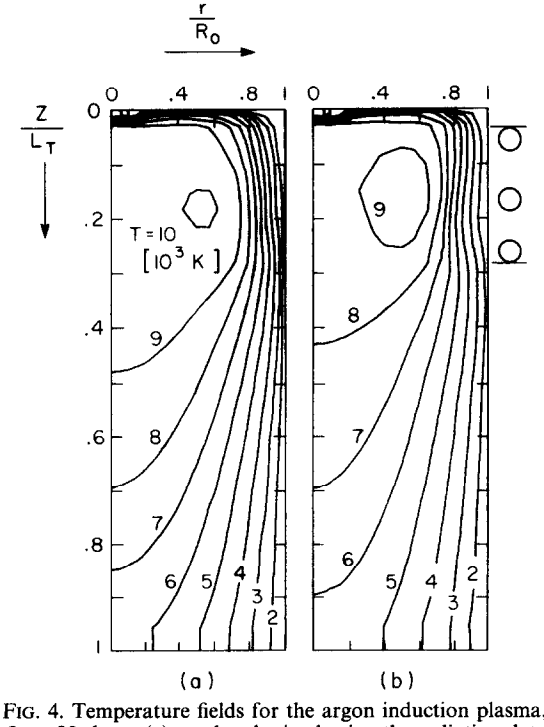


FIG. 4. Temperature fields for the argon induction plasma, $Q_0 = 20$ slpm: (a) results obtained using the radiation data by Mensing and Boedeker [12] and Evans and Tankin [13]; (b) results obtained using the radiation data by Cram [6].

as a function of the total plasma gas flow rate, $Q_0$. In both cases, the total radiation loss from the plasma, $Q_R$, is relatively insensitive to variations of the total plasma gas flow rate. A comparison of Figs. 5(a) and (b) shows, however, that Cram's [6] radiation data gives rise to total radiative energy losses which are higher by almost 20% of the total plasma power, compared to that obtained using the data of Mensing and Boedeker [12] and Evans and Tankin [13]. Wall conductive losses, $Q_w$, and the enthalpy of the gas at the exit of the plasma confinement tube, $Q_g$, are indirectly affected by the radiation data used and are generally lower using Cram's [6] data because of the overall decrease of the temperature level of the plasma. Because of the dependence of these energy balance data on the physical dimensions of the plasma and in particular on the length of the plasma confinement tube used, $L_t$, they should be considered only in relative terms keeping in mind that $L_t = 250$ mm in the present case.

### 4.2. *Influence of copper vapor on the radiative losses*

In the processing of metallic powders in an induction r.f. plasma, the interaction between the plasma and the particles can have a major influence on the overall process. Momentum and thermal loading effects have been previously studied [3]. An analysis of the volumetric emission of atmospheric argon

plasmas (Fig. 2), shows a substantial increase in the plasma emission in the presence of even small concentrations of copper vapor. Although, melting and evaporation of metallic powders have been the subject of considerable research in thermal plasma devices, the effect of the presence of metallic vapors has so far been generally overlooked.

In the present analysis of the effect of metallic vapors on the temperature field in an induction plasma, four cases are considered.

In the first two cases (cases (A-1) and (A-2)) a fine copper powder ($\bar{d}_p = 30$ $\mu$m, $\sigma = 3$ $\mu$m) is axially injected into the plasma at a mass feed rate of $\dot{m}_p = 1.0$ g min$^{-1}$. The powder carrier gas flow rate is set at $Q_1 = 4.0$ slpm while the plasma and sheath gas streams are set at $Q_2 = 3.0$ and $Q_3 = 33.0$ slpm, respectively. Cases (B-1) and (B-2) are for essentially the same conditions except for the increase of the powder feed rate to $\dot{m}_p = 10$ g min$^{-1}$. The length of the plasma confinement tube in all four cases is 500 mm.

For cases (A-1) and (B-1), computations are carried out using the radiation data for pure argon after Cram [6] given in Fig. 2. The effect of the presence of the copper vapor on the total radiative power of the plasma is taken into account in cases (A-2) and (B-2) using the data by Cram [6] given in Fig. 2. These give the volumetric specific emission of the plasma, $Q_r$, as a function of temperature and the mass fraction of copper vapor.

The computed temperature fields in the discharge for each of cases (A-1) and (A-2) are given in Fig. 6. Figure 6(a) gives the temperature isotherms obtained using the radiation data for pure argon, while Fig. 6(b) gives the corresponding temperature isotherms taking into account the effect of the presence of the copper vapor on the specific emission of the plasma. Because of the axial mode of injection of the copper powder in the plasma, the off-axis maximum temperature region of the discharge is not affected by the presence of the copper powder or the effect of the copper vapor on the radiation properties of the plasma. The situation is, however, completely different in the central region which has a much higher concentration of copper vapor as shown by the concentration isocontours given in Fig. 7.

Figure 8 shows the axial temperature profile along the centerline of the discharge for each of these four cases (cases (A-1), (A-2), (B-1) and (B-2)) with the dotted lines indicating the temperature profile obtained using the radiation data of pure argon only, while the solid lines correspond to that obtained taking into account the increased emission power of the plasma in the presence of the copper vapor. The effect is particularly important for cases (A-1) and (A-2) with $\dot{m}_p = 1.0$ g min$^{-1}$. The observed drop of the maximum temperature of the plasma along the axis of the discharge by more than 4000 K is due to the radiative energy loss mechanism.

The qualitative increase of the brightness of the plasma normally observed in the laboratory, in the presence of metal vapors, is obviously a direct consequence of the increase of the specific emission of the

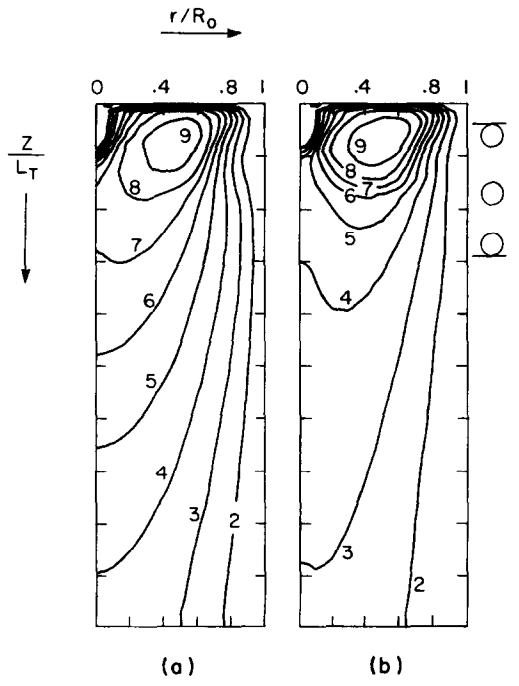


FIG. 6. Temperature fields for an argon plasma in the presence of copper powder, $\dot{m}_p = 1.0$ g min$^{-1}$: (a) results obtained using the radiation data for pure argon [6]; (b) results obtained using the radiation data for Ar/Cu mixtures [6].

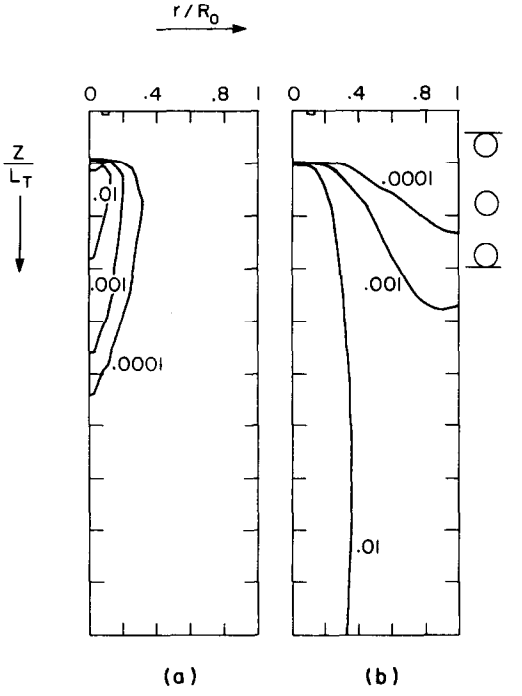


FIG. 7. Isocontours of the mass fraction of the copper vapor in the plasma, $\dot{m}_p = 1.0$ g min$^{-1}$: (a) results obtained using the radiation data for pure argon [6]; (b) results obtained using the radiation data for Ar/Cu mixtures [6].

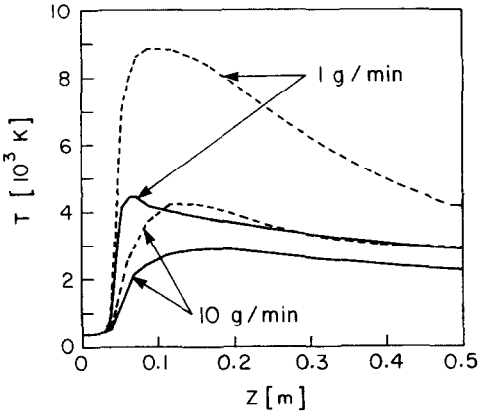


FIG. 8. Axial temperature profile along the centerline of the discharge in the presence of copper powder: $\dot{m}_p$ = 1.0 and 10.0 g min$^{-1}$. – – – –, radiation data for pure argon; ——, radiation data for Ar/Cu mixtures [6].

plasma gas. The effect is demonstrated in Fig. 9 by the substantial increase of the region where the plasma has an emission power higher than $10^5$ W m$^{-3}$. Figure 9(a) gives the emission isocontours obtained using the radiation data for pure argon while, Fig. 9(b) gives the corresponding isocontours taking into account the effect of the presence of the metal vapor on the volumetric emission from the plasma.

Due to the strong interaction between the plasma temperature field and the temperature history of the individual copper particles injected into the discharge,

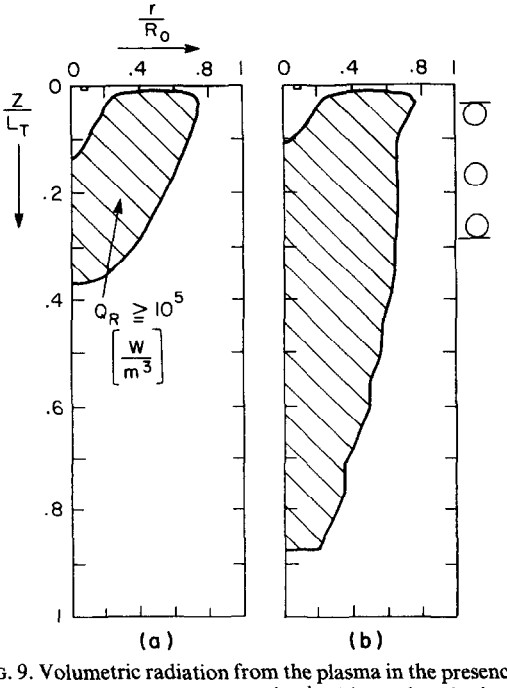


FIG. 9. Volumetric radiation from the plasma in the presence of copper vapor, $\dot{m}_p$ = 1.0 g min$^{-1}$: (a) results obtained using the radiation data for pure argon [6]; (b) results obtained using the radiation data for Ar/Cu mixtures [6].

Table 2. Effect of copper vapor radiation on the energy exchange between the plasma and the particles and the fraction of the powder vaporized

| Powder feed rate, $\dot{m}_p$ (g min$^{-1}$) | Case | $Q_E$ (W) | % evap. (w) |
|---|---|---|---|
| 1.0 | A-1 | 90 | 100.0 |
| | A-2 | 74 | 42.0 |
| 10.0 | B-1 | 529 | 15.0 |
| | B-2 | 367 | 1.7 |

the local cooling of the plasma caused by the increase of radiative energy losses will be accompanied by a drop in the heat exchange between the plasma and the injected powder. Table 2 gives the total energy exchange between the plasma and the particles, $Q_E$, and the fraction of the mass of the injected copper powder which is vaporized (% evap.) in the plasma for the two powder feed rates investigated, $\dot{m}_p$ = 1.0 and 10.0 g min$^{-1}$. Separate values are given, depending on whether the computations are carried out using the radiation properties of pure argon (cases (A-1) and (B-1)) or that of Ar/Cu vapor mixtures (cases (A-2) and (B-2)).

It may be noted that the local radiative cooling of the plasma is responsible for the decrease of the energy exchange between the plasma and the particles by 18% at $\dot{m}_p$ = 1 g min$^{-1}$ and by more than 30% at $\dot{m}_p$ = 10 g min$^{-1}$. The percentage of the powder vaporized is also noted to decrease considerably from 100% of the feed powder at $\dot{m}_p$ = 1.0 g min$^{-1}$, neglecting the metal vapor radiation effects, to only 42% of the powder feed when the metal vapor radiation is taken into account. A corresponding decrease in the percentage vaporization of the powder is also observed at $\dot{m}_p$ = 10.0 g min$^{-1}$ depending on whether metal vapor radiation is taken into account or not.

## 5. SUMMARY AND CONCLUSION

The present study has shown that in induction plasma modelling the computed temperature fields can be rather sensitive to the radiation data used. Variations between available radiation data for argon at atmospheric pressure can be responsible for differences as large as 1000 K in the computed temperature fields in the discharge.

The considerable increase of the emission power of a plasma in the presence of metal vapors results in the local cooling of the plasma and a reduction in its ability to melt and vaporize metal particles even at relatively low powder feed rates.

*Acknowledgment*—The financial support of the Natural Science and Engineering Research Council of Canada, and of the Fonds pour la Formation de Chercheurs et l'Aide à la Recherche du Québec are gratefully acknowledged.

## REFERENCES


1. W. H. Gauvin, *Plasma Chem. Plasma Process.* **9,** 65s (1989).
2. J. Jurewicz, C. Lemire, A. Czernichowski and M. I. Boulos, ISPC-8, Tokyo, Japan (1987).
3. P. Proulx, J. T. Mostaghimi and M. I. Boulos, *Int. J. Heat Mass Transfer* **28,** 1327 (1985).
4. J. T. Mostaghimi, P. Proulx and M. I. Boulos, *Plasma Chem. Plasma Process.* **4,** 129 (1984).
5. H. W. Emmons, *Physics Fluids* **10,** 1125 (1967).
6. L. E. Cram, Private communication (1987).
7. C. H. Kruger, ISPC-9, Pugnochiuso, Italy (1989).
8. D. Wei, B. Farouk and D. Apelian, *Met. Trans. B* **19B,** 213 (1988).
9. J. T. Mostaghimi and M. I. Boulos, *Plasma Chem. Plasma Process.* **9,** 25 (1989).
10. A. Essoltani, P. Proulx, M. I. Boulos and A. Gleizes, *J. Analyt. Atom. Spectrom.* **5,** 543 (1990).
11. C. T. Crowe, M. P. Sharma and D. E. Stock, *J. Fluids Engng* **99,** 325 (1977).
12. A. E. Mensing and L. R. Boedeker, NASA-CR-1312 (1969).
13. D. L. Evans and R. S. Tankin, *Physics Fluids* **10,** 1137 (1967).
14. A. Kanzawa and I. Kimura, *AIAA J.* **5,** 1315 (1967).


## APPENDIX A. PLASMA FLOW, TEMPERATURE, CONCENTRATION AND ELECTROMAGNETIC FIELD EQUATIONS AND BOUNDARY CONDITIONS

The definitions of all the symbols used are given in the Nomenclature.

A.1. *The plasma equations*

A.1.1. *Continuity.*

$$\frac{1}{r}\frac{\partial}{\partial r}(r\rho v)+\frac{\partial}{\partial z}(\rho u)=S_{\mathrm{p}}^{\mathrm{c}}. \tag{A1}$$

A.1.2. *Momentum transfer equations.*

$$\rho\left\{v\frac{\partial u}{\partial r}+u\frac{\partial u}{\partial z}\right\}=-\frac{\partial p}{\partial z}+2\frac{\partial}{\partial z}\left(\mu\frac{\partial u}{\partial z}\right)+\frac{1}{r}\frac{\partial}{\partial r}\left\{\mu r\left(\frac{\partial v}{\partial r}+\frac{\partial u}{\partial r}\right)\right\}+\rho g \tag{A2}$$

$$\rho\left\{v\frac{\partial v}{\partial r}+u\frac{\partial v}{\partial z}\right\}=-\frac{\partial p}{\partial r}+\frac{2}{r}\frac{\partial}{\partial r}\left(\mu r\frac{\partial v}{\partial r}\right)+\frac{\partial}{\partial z}\left\{\mu\left[\frac{\partial v}{\partial z}+\frac{\partial u}{\partial r}\right]\right\}-\frac{2\mu v}{r^2}+Fr. \tag{A3}$$

A.1.3. *Energy transfer equation.*

$$\rho\left(v\frac{\partial h}{\partial r}+u\frac{\partial h}{\partial z}\right)=\frac{1}{r}\frac{\partial}{\partial r}\left(r\frac{k}{c_p}\frac{\partial h}{\partial r}\right)+\frac{\partial}{\partial z}\left(\frac{k}{c_p}\frac{\partial h}{\partial z}\right)+P-Q_{\mathrm{r}}+S_{\mathrm{p}}^{\mathrm{E}}. \tag{A4}$$

A.1.4. *Mass transfer equation.*

$$\rho\left(v\frac{\partial y}{\partial r}+u\frac{\partial y}{\partial z}\right)=\frac{1}{r}\frac{\partial}{\partial r}rD\frac{\partial y}{\partial r}+\frac{\partial}{\partial z}\left(D\frac{\partial y}{\partial z}\right)+S_{\mathrm{p}}^{\mathrm{c}}. \tag{A5}$$

A.2. *Electromagnetic field equations*

$$\frac{1}{r}\frac{\mathrm{d}}{\mathrm{d}r}(rE_\theta)=-\zeta\omega H_z\sin x \tag{A6}$$

$$\frac{\mathrm{d}H_z}{\mathrm{d}r}=-\sigma E_\theta\cos x \tag{A7}$$

$$\frac{\mathrm{d}\chi}{\mathrm{d}r}=\frac{\sigma E_\theta}{H_z}\sin\chi-\frac{\zeta\omega H_z}{E_\theta}\cos\chi \tag{A8}$$

with $P=\sigma E_\theta^2$ the volumetric rate of heat generation due to Joule heating and $Fr=-\zeta\sigma E_\theta H_z\cos\chi$ the radial body force acting on the plasma gas in the discharge region.

A.3. *Boundary conditions*

Inlet conditions ($z=0$)

$$v=0$$

$$u=\begin{cases}Q_1/\pi r_1^2 & r<r_1\\ 0.0 & r_1\leqslant r\leqslant r_2\\ Q_2/\pi(r_3^2-r_2^2) & r_2<r\leqslant r_3\\ Q_3/(R_0^2-r_3^2) & r_3<r\leqslant R_0\end{cases} \tag{A9}$$

$$T=350\ \mathrm{K}$$

$$y=0.$$

Centerline ($r=0$)

$$v=0$$

$$\frac{\partial u}{\partial r}=0$$

$$\frac{\partial h}{\partial r}=0$$

$$\frac{\partial y}{\partial r}=0. \tag{A10}$$

Wall ($r=R_0$)

$$u=v=0$$

$$\frac{k}{c_p}\frac{\partial h}{\partial r}=\frac{k_{\mathrm{c}}}{\delta_{\mathrm{w}}}(T-T_{\mathrm{w0}})$$

$$\frac{\partial y}{\partial r}=0 \tag{A11}$$

where $T_{\mathrm{w0}}$ is the external surface temperature of the tube ($T_{\mathrm{w0}}=350$ K).

Exit ($z=L_{\mathrm{t}}$). The boundary condition at this section is not known. However, if the exit Peclet number, i.e. ($Re\cdot Pr$) is sufficiently large, one can safely assume the following:

$$\frac{\partial h}{\partial z}=0$$

$$\frac{\partial v}{\partial z}=0$$

$$\frac{\partial(\rho u)}{\partial z}=0$$

$$\frac{\partial y}{\partial z}=0. \tag{A12}$$

The boundary conditions for the electromagnetic field are set at $r=0$ and $L_1\leqslant z\leqslant L_2$

$$\chi=\frac{\pi}{2}$$

$$E_\theta=0$$

$$H_z=H_{\mathrm{c}\infty}\left\{\frac{L_2-z}{[R_{\mathrm{c}}^2+(L_2-z)^2]^{1/2}}-\frac{L_2-z}{[R_{\mathrm{c}}^2+(L_2-z)^2]^{1/2}}\right\} \tag{A13}$$

where $H_{\mathrm{c}\infty}$ is the magnetic field intensity for an infinite solenoid

$$H_{\mathrm{c}\infty}=\frac{NI}{L_2-L_1}. \tag{A14}$$

It is to be noted that $H_{\infty\infty}$ is not specified, rather the total power input to the plasma $P_0$, is known. This is set as an integral type boundary condition

$$P_t = \int_{z=L_1}^{L_2} \int_{r=0}^{R_0} 2\pi P \, dr \, dz \tag{A15}$$

and if $P_t \neq P_0$, a correction factor to the electric and magnetic fields is found

$$\alpha_c = \sqrt{\left(\frac{P_0}{P_t}\right)}. \tag{A16}$$

Multiplying the electromagnetic fields by $\alpha_c$ insures that the condition $P_t = P_0$ is satisfied.

## APPENDIX B. PARTICLE TRAJECTORY, THERMAL HISTORY, AND PLASMA–PARTICLE COUPLING

The definitions of all the symbols used are given in the Nomenclature.

The single particle trajectory equations are given as

$$\frac{du_p}{dt} = -\tfrac{3}{4} C_d \left(\frac{\rho}{\rho_p d_p}\right)(u-u_p)U_r + g \tag{B1}$$

$$\frac{dv_p}{dt} = -\tfrac{3}{4} C_d \left(\frac{\rho}{\rho_p d_p}\right)(v-v_p)U_r \tag{B2}$$

with

$$U_r = [(u-u_p)^2 + (v-v_p)^2]^{1/2}. \tag{B3}$$

The drag coefficient $C_d$ is determined from the following equations, with $Re_p = \rho U_r d_p/\mu$:

$$C_d = \frac{24}{Re_p} \qquad Re_p < 0.2$$

$$C_d = \frac{24}{Re_p}\left(1 + \frac{3}{16} Re_p\right) \qquad 0.2 < Re_p < 2$$

$$C_d = \frac{24}{Re_p}(1 + 0.11 Re_p^{0.81}) \qquad 2 < Re_p < 20$$

$$C_d = \frac{24}{Re_p}(1 + 0.189 Re_p^{0.632}) \qquad 20 < Re_p. \tag{B4}$$

The thermal history of the particles is calculated from

$$Q_p = h_c A_p (T - T_p) - \sigma \varepsilon_p A_p (T_p^4 - T_a^4) \tag{B5}$$

with

$$Q_p = \tfrac{1}{6}\rho\pi d_p^3 c_{ps} \frac{dT_p}{dt} \qquad T < T_m \tag{B6}$$

$$Q_p = \tfrac{1}{6}\rho\pi d_p^3 c_{pl} \frac{dT_p}{dt} \qquad T_m < T < T_v \tag{B7}$$

$$Q_p = \tfrac{1}{6}\rho\pi d_p^3 H_m \frac{dX_p}{dt} \qquad T = T_m \tag{B8}$$

$$Q_p = -\tfrac{1}{2}\rho\pi d_p^2 H_v \frac{dd_p}{dt} \qquad T = T_v. \tag{B9}$$

The heat transfer coefficient, $h_c$, for an argon plasma at atmospheric pressure is given by

$$\frac{h_c d_p}{k} = 2.0 + 0.515 Re_p^{0.5}. \tag{B10}$$

The following terms are the so-called plasma–particle coupling terms [3]. Only the energy and the mass coupling terms are taken into account

$$S^E_{p_{i,j}} = \sum_{k=1}^{n_d} \sum_{l=1}^{n_r} C^{l,k}(\bar{Q}_p^{l,k} + \bar{Q}_v^{l,k}) \tag{B11}$$

$$S^c_{p_{i,j}} = \sum_{k=1}^{n_d} \sum_{l=1}^{n_r} C^{l,k} \frac{\Delta m_p^{l,k}}{\tau^{l,k}}. \tag{B12}$$

## TRANSFERT D'ENERGIE RADIATIVE DANS LA MODELISATION D'UN PLASMA

**Résumé**—L'influence de pertes d'énergie radiative sur les champs de vitesse et de température d'un plasma couplé par induction à une fréquence radio est étudiée dans le cas d'un plasma d'argon pur et pour un plasma d'argon en présence d'une faible concentration de vapeur de cuivre. Un modèle mathématique permet de calculer les champs de vitesse et de température en utilisant différentes données de source radiative pour un gaz de plasma en fonction de la température. Les résultats montrent que les variations entre différents groupes de données peuvent avoir un effet sensible sur les champs de température calculés. La présence de faibles concentrations de vapeurs métalliques est responsable du refroidissement local du plasma à cause de l'accroissement des pertes d'énergie radiative.

## MODELLIERUNG DES STRAHLUNGSWÄRMEAUSTAUSCHES IN PLASMASTRÖMEN

**Zusammenfassung**—Der Einfluß des Strahlungswärmeverlustes auf das Strömungs- und Temperaturfeld eines Plasmas unter dem Einfluß einer Radiofrequenz wird für reines Argon-Plasma und ein durch geringe Konzentrationen von Kupferdampf verunreinigtes Argon-Plasma untersucht. Es wird ein mathematisches Modell zur Berechnung des Temperatur- und Strömungsfeldes verwendet, wobei in Abhängigkeit von der Plasmatemperatur die Daten für die Wärmestrahlung unterschiedlich sind. Die Ergebnisse zeigen, daß diese unterschiedlichen Daten einen wesentlichen Einfluß auf die berechnete Temperaturverteilung haben. Es zeigt sich weiter, daß geringe Konzentrationen von Metalldampf durch wesentlich erhöhte Strahlungswärmeverluste zu einer lokalen Abkühlung führen.

## ПЕРЕНОС ЭНЕРГИИ ИЗЛУЧЕНИЯ В МОДЕЛИ ИНДУКЦИОННОЙ ПЛАЗМЫ

**Аннотация**—Исследуется влияние потерь энергии излучения на поля течения и температуры плазмы, возбужденной радиочастотным полем, в случаях чистой плазмы аргона и плазмы аргона с наличием малых концентраций паров меди. Для расчета полей течения и температуры применяется математическая модель, в которой используются данные для различных источников излучения плазменного газа в виде функции температуры. Полученные результаты свидетельствуют о том, что различия между наборами данных, используемых при расчетах, могут оказывать значительное влияние на температурные поля. Показано, что наличие малых концентраций паров металлов вызывают локальное охлаждение плазмы за счет существенного увеличения потерь энергии излучением.